

Time delay interferometry and principal component analysis for noise cancellation of TianQin

Xinchun Hu(胡新春) and Yan Wang(王炎)
Citation: Chin. Phys. B, 2026, 35 (**5**): 050401. DOI: 10.1088/1674-1056/ae12d4
http://cpb.iphy.ac.cn; http://iopscience.iop.org/cpb

What follows is a list of articles you may be interested in

Probing the shape of the primordial curvature power spectrum and the energy scale of reheating with pulsar timing arrays

Lele Fan(范乐乐), Jie Zheng(郑捷), Fengge Zhang(张丰阁), and Zhi-Qiang You(尤志强)
Chin. Phys. B, 2025, 34 (**2**): 020402. DOI: 10.1088/1674-1056/ad9a98

Detecting short-term gravitational waves from post-merger hyper-massive neutron stars with a kilohertz detector

Yikang Chen(陈奕康) and Zong-Hong Zhu(朱宗宏)
Chin. Phys. B, 2024, 33 (**8**): 080401. DOI: 10.1088/1674-1056/ad5320

Application of Newtonian approximate model to LIGO gravitational wave data processing

Jie Wu(吴洁), Jin Li(李瑾), and Qing-Quan Jiang(蒋青权)
Chin. Phys. B, 2023, 32 (**9**): 090401. DOI: 10.1088/1674-1056/acd8a3

Simulation of the gravitational wave frequency distribution of neutron star-black hole mergers

Jianwei Zhang(张见微), Chengmin Zhang(张承民), Di Li(李荻), Xianghan Cui(崔翔翰), Wuming Yang(杨伍明), Dehua Wang(王德华), Yiyan Yang(杨佚沿), Shaolan Bi(毕少兰), and Xianfei Zhang(张先飞)
Chin. Phys. B, 2021, 30 (**12**): 120401. DOI: 10.1088/1674-1056/abff28

High-frequency gravitational waves having large spectral densities and their electromagnetic response

Li Fang-Yu (李芳昱), Wen Hao (文毫), Fang Zhen-Yun (方祯云)
Chin. Phys. B, 2013, 22 (**12**): 120402. DOI: 10.1088/1674-1056/22/12/120402

Time delay interferometry and principal component analysis for noise cancellation of TianQin

Xinchun Hu(胡新春)[1,†] and Yan Wang(王炎)[2]

[1] *School of Electrical and Information Engineering, Tongling University, Tongling* 244000, *China*
[2] *National Gravitation Laboratory, MOE Key Laboratory of Fundamental Physical Quantities Measurements, Department of Astronomy and School of Physics, Huazhong University of Science and Technology, Wuhan* 430074, *China*

(Received 27 July 2025; revised manuscript received 24 September 2025; accepted manuscript online 14 October 2025)

TianQin is a proposed space-borne laser interferometer which aims to detect gravitational waves in the low frequency band (10^{-4} Hz–10^{0} Hz). However, for space-borne interferometry detectors the laser phase noise is expected to be 7–8 orders of magnitude higher than the gravitational wave signals, due to unequal and time-varying arm lengths. Time delay interferometry (TDI) is an effective method to cancel laser phase noise by synthesizing virtual equal arm interferometric measurements with time delayed Doppler data combinations. In previous work it has been shown that TDI variables can also be understood within the context of principal component analysis (PCA), as combinations of eigenvectors of the total noise covariance matrix. It is therefore possible to generate the same TDI variables using a PCA approach – by computing the eigenvectors of the noise covariance matrix at a specific time. In this paper we extend significantly the previous work on a PCA approach to generating TDI variables by presenting TDI sensitivity curves for TianQin approximated as both a static and moving constellation of satellites. We compare the covariance matrix for the static and moving case, from the point of view of performing statistical inference using PCA. We also demonstrate the equivalency between the 'conventional' second generation TDI variables and those obtained using PCA.

Keywords: gravitational waves, time delay interferometry, principal component analysis

PACS: 04.30.–w, 04.80.Nn, 04.20.Cv

DOI: 10.1088/1674-1056/ae12d4 **CSTR:** 32038.14.CPB.ae12d4

1. Introduction

The detection of gravitational waves (GWs) by Laser Interferometer Gravitational-Wave Observatory (LIGO) and Virgo have opened the era of GW astronomy. The ground-based detectors, such as Advanced LIGO.[1,2] Advanced Virgo[3] and KAGRA[4] are all operating in the high frequency band (10–10^4) Hz. It can detect compact binary mergers (stellar-mass binary black hole mergers, binary neutron star mergers, neutron star black hole mergers), core collapse supernova and so on. For low frequency band (10^{-4}–10^{-1}) Hz, super massive black hole binaries (SMBHBs), extreme mass ratio inspirals (EMRIs) and galactic white dwarf binaries (GWDBs) are expected detect by space-borne detectors. LISA/eLISA[5,6] is the most well studied concept so far, especially with the successful demonstration of the gravity reference system and space laser interferometry by the LISA Pathfinder mission.[7] Several Earth-orbiting gravitational-wave detectors have also been proposed, such as TianQin,[8] LAGRANGE,[9] g-LISA/GEOGRAWI,[10,11] and OMEGA.[12] Furthermore, various other solar-orbiting detectors have also been suggested, such as ASTROD-GW,[13,14] Taiji (ALIA descoped),[15] Big Bang Observer,[16,17] and DECIGO.[18] All of these missions are currently at various stages of research and development. A thorough overview of space-borne GW detectors can be found in Ref. [19].

The successful detection of GWs made so far have been achieved with equal arm-length of ground-based interferometers. On the other hand, for unequal arm-length spaceborne detectors, e.g., LISA[20] and TianQin,[8] the laser phase noise is the dominate noise source and it needs to be removed first. Time delay interferometry (TDI)[21] is a technique designed to achieve this by synthesizing different Doppler data combinations to increase the symmetry of the optical paths followed by the laser light, which can greatly reduce the effect of laser phase noise.

A lot of previous work were devoted to analyze the sensitivity curves of space-based detectors with TDI. The first application of TDI[22] was proposed under the assumption of a static constellation (or a constellation with time-independent but equal arm lengths) — a configuration that is also called the first generation TDI. Armstrong *et al.*[23] gave the sensitivity curves for different laser-noise-cancelling data combinations based on a simplified space-borne detector. Estabrook *et al.*[24] considered a more complex configuration of the LISA constellation, where each spacecraft has two optical benches. This work modified the original TDI scheme to eliminate the noise due to the optical bench motions. A modified noise power spectral density for different data combinations and the

†Corresponding author. E-mail: 030261@tlu.edu.cn

© 2026 Chinese Physical Society and IOP Publishing Ltd. All rights, including for text and data mining, AI training, and similar technologies, are reserved.

details of the algebra for a realistic sensitivity curve were generalized in Ref. [25]. For more discussion on the construction and application of LISA TDI variables, one can refer to Refs. [24,26–36].

A different approach to TDI called principle component analysis (PCA) was first presented in Romano and Woan,[37] who examined the problem of reducing the laser noise for LISA in the context of Bayesian inference. PCA[38] is a general statistical technique used to identify set of uncorrelated variables by analyzing eigenvalues and eigenvectors of the noise covariance matrix of the space-borne detector. Romano and Woan applied this PCA technique to a simplified illustrative model of the LISA data streams, aiming to simplified the likelihood function. They found that PCA identified a linear combination of the datastreams that did not depend on the laser noise that was common to different spacecraft, thereby equivalent to TDI method. However, this analysis is on the first generation TDI. Thereafter, Michele Dawn[39] extended the PCA method to more realistic LISA data analysis including all phase-locked, phase-locked on each spacecraft, and not locked cases. Data analysis for space-borne detectors based TDI variables, such as mock LISA data challenge, is a more realistic data analysis demonstration. More recently, Baghi *et al.*[40] employed an asymptotic formulation of the delay operators to formalize the PCA approach in the frequency domain. They[41] also demonstrated that PCA can eliminate laser frequency noise without any prior knowledge.

In this work, we calculate the sensitivity curve for different combinations of TDI data from an Earth-orbiting space-borne detector (TianQin). The most important contribution is we firstly give the sensitivity curve of a moving detector and compare it with static one. From the perspective of statistic inference, we obtain the noise covariance matrix of both static and moving detectors using the PCA method. In fact, TDI is a consequence of PCA and we prove this relation based on the second generation TDI using a toy model.

The rest of the paper is organized as follows. In Section 2, we present the principle and notation for time delay interferometry, which are then used in the calculation of sensitivity curve for TDI combinations including static and moving TianQin detector, respectively in Section 3. Statistic inference demonstration based on PCA is given in Section 4. The relationship between PCA and the second generation TDI is discussed in Section 5. We conclude the main part of the paper in Section 6.

2. Time delay interferometry

Time delay interferometry is a technique to cancel laser phase noise by using different Doppler data combinations with different time delays. The simplified configuration for a triangular space-borne detector is showed in Fig. 1. We follow the notation and conventions as Ref. [24]. The spacecrafts are labelled as 1, 2, and 3, and interferometric arms are labelled as the index of opposite spacecraft, L_1, L_2, and L_3. We denote the detector guiding center as O. Relative to O, the spacecrafts are joint by coplanar unit vector $\hat{p}_1$, $\hat{p}_2$, and $\hat{p}_3$. $\hat{n}_1$, $\hat{n}_2$, $\hat{n}_3$ are unit vectors along the lines connecting spacecrafts paris. y_{ij} is the Doppler data received by the phase meter at the spacecraft j, which was transmitted along the arm i. The delayed data stream is expressed as $y_{ij,k} = y_{ij}(t - L_k)$. The detector response to a transverse-traceless plane GW response for one-way Doppler data series can be expressed as

$$\begin{aligned} y_{31}^{\rm gw} &= \left[1 + \frac{l}{L_3}(\hat{k}\cdot\hat{p}_1 - \hat{k}\cdot\hat{p}_2)\right] \\ &\quad \times [\Psi_3(t - \hat{k}\cdot\hat{p}_2 l - L_3) - \Psi_3(t - \hat{k}\cdot\hat{p}_1 l)], \\ y_{21}^{\rm gw} &= \left[1 - \frac{l}{L_2}(\hat{k}\cdot\hat{p}_3 - \hat{k}\cdot\hat{p}_1)\right] \\ &\quad \times [\Psi_2(t - \hat{k}\cdot\hat{p}_3 l - L_2) - \Psi_2(t - \hat{k}\cdot\hat{p}_1 l)], \end{aligned} \tag{1}$$

where Ψ_i is

$$\Psi_i(t) = \frac{1}{2}\frac{\hat{n}_i\cdot\boldsymbol{h}(t)\cdot\hat{n}_i}{1-(\hat{k}\cdot n_i)^2}, \tag{2}$$

where $\hat{k}$ is the direction of propagation GW, l is the distance between detector guiding center and each spacecraft. We can also obtain the relation $l(\hat{p}_2 - \hat{p}_3) = L\hat{n}_1$ from this configuration. Four other one-way Doppler data relations for gravitational wave at vertices 2 and 3 can be obtained by cyclic permutation of indices as Eqs. (1).

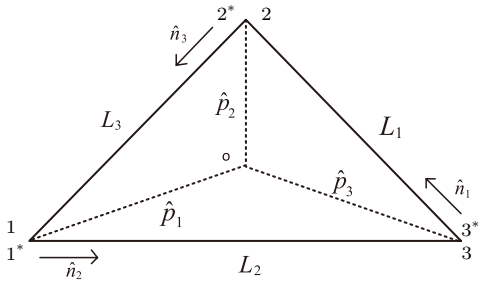


Fig. 1. Static configurations for space-borne detector. The guiding center is labelled as O. Spacecrafts at each vertex are labelled as 1, 1* for the case that there is no phase-locking at each spacecraft, etc. In this work, we can take each vertex for one index when phase-locking at each spacecraft for simplification.

Doppler data includes gravitational wave $y_{ij}^{\rm gw}(t)$, laser phase noise $p(t)$, the secondary noise $n(t)$ (here, for illustrative purpose we consider the secondary noise include proof mass acceleration noise and the optical path noise) and other noise that we ignored here, e.g., $y_{ij}(t) = y_{ij}^{\rm gw}(t) + p(t) + n(t)$. There are five commonly used types of first-generation TDI data combinations[23,24]

$$\alpha = y_{21} + y_{13,2} + y_{32,12} - y_{31} - y_{12,3} - y_{23,13}, \tag{3}$$

$$\begin{aligned} X &= y_{32,322} + y_{31,22} + y_{23,2} + y_{21} \\ &\quad - y_{23,233} - y_{32,3} - y_{21,33} - y_{31}, \end{aligned} \tag{4}$$

$$P = y_{23,311}+y_{12,13}+y_{13,3}+y_{32,2} - y_{32,211}-y_{13,12}-y_{12,2}-y_{23,3}, \quad (5)$$

$$E = y_{12,21}+y_{13,2}+y_{31,11}+y_{21}-y_{13,31} - y_{12,3}-y_{21,11}-y_{31}, \quad (6)$$

$$U = y_{21,113}+y_{32,11}+y_{13,1}+y_{12} - y_{12,123}-y_{13,23}-y_{21,3}-y_{32}. \quad (7)$$

Assuming that laser noise has been effectively suppressed below the secondary noises via TDI, we can substitute proof mass acceleration noise and optical path noise into the above expressions to obtain the remaining power spectrum density for each data combination. The resulting noise power spectrum density for combination α, X, P, E, and U are[24]

$$S_\alpha(f) = [8\sin^2(3\pi fL)+16\sin^2(\pi fL)]S_y^{\rm pm}+6S_y^{\rm op}, \quad (8)$$

$$S_X(f) = [8\sin^2(4\pi fL)+32\sin^2(2\pi fL)]S_y^{\rm pm} + 16\sin^2(2\pi fL)S_y^{\rm op}, \quad (9)$$

$$S_P(f) = [8\sin^2(2\pi fL)+32\sin^2(\pi fL)]S_y^{\rm pm} + [8\sin^2(2\pi fL)+8\sin^2(\pi fL)]S_y^{\rm op}, \quad (10)$$

$$S_E(f) = [32\sin^2(\pi fL)+8\sin^2(2\pi fL)]S_y^{\rm pm} + [8\sin^2(\pi fL)+8\sin^2(2\pi fL)]S_y^{\rm op}, \quad (11)$$

$$S_U(f) = [16\sin^2(\pi fL)+8\sin^2(2\pi fL) + 16\sin^2(3\pi fL)]S_y^{\rm pm} + [4\sin^2(\pi fL)+8\sin^2(2\pi fL) + 4\sin^2(3\pi fL)]S_y^{\rm op}. \quad (12)$$

Here we assume the arm lengths $L = L_1 = L_2 = L_3$ for TianQin. $S_y^{\rm pm}$ is power spectrum density of proof mass acceleration noise and $S_y^{\rm op}$ is power spectrum density of optical path noise of TianQin. The quantitative details of those items can refer to Ref. [8].

In order to suppress the laser frequency noise, the orbit design requires the orbit of the spacecraft to be a near circular orbit. The analytic orbit used in this work accounts for perturbations solely from the Sun and the Earth for TianQin. Laser frequency noise $(\delta f/f_l)$ coupled to the mismatch (ΔL) between the two arm lengths of the interferometer leads to a noise $\delta x_{\rm FN} = (\delta f/f_l)\Delta L$. Assuming $\Delta L = 0.01\ L$, a frequency noise below $\delta f \lesssim 0.1$ mHz/Hz$^{1/2}$ is required for TianQin. This is to be achieved first by using an on-board frequency stabilization system to reach better than 10 Hz/Hz$^{1/2}$, and then by using the time-delay interferometry to reach 0.1 mHz/Hz$^{1/2}$. This requires the asymmetric arm length of the TDI combination to be less than 4.7×10^{-8} s. We simulated all TDI combinations to make it meet the requirements of laser frequency noise suppression. The eccentricity of spacecraft orbit should less than $e < 0.003$ for all data combinations. All results show as follow in Fig. 2. Where TDI combination P has the same noise power spectral density as the combination E. Six-link data combination of the first-generation TDI α can not reach this requirement because of Sagnac effect. We give the arm-length residual for the second-generation α_1 in Fig. 3. The similar results for numerical orbit of ASTROD can refer to Ref. [42].

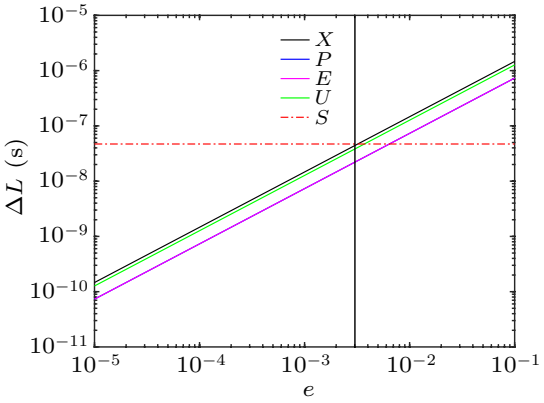


Fig. 2. The arm length residuals as a function of spacecraft orbit eccentricity for different TDI data combinations. Here S stands for the standard value that TDI should satisfy for suppressing laser frequency noise.

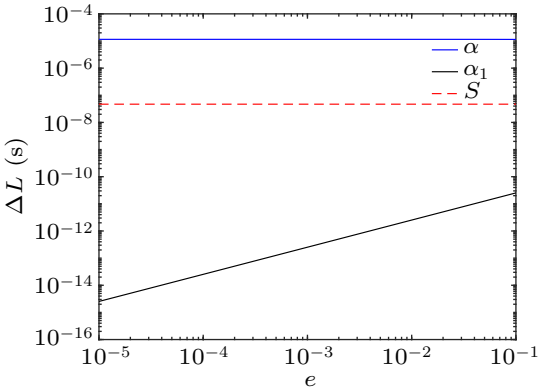


Fig. 3. The arm length residuals as a function of spacecraft orbit eccentricity for the first-generation and second-generation α.

The laser noise spectral density[30] can be evaluated by

$$S_i^l(f) = \left(\frac{\delta f}{f_l}\right)^2 (2\pi f)^2(\delta t)^2. \quad (13)$$

Here i represents different TDI data combinations, the laser frequency $f_l = 2.82\times10^{14}$ Hz. We give a comparison of noise power spectral density between the secondary noise and laser frequency noise. All the above, we proof that the laser frequency noise can be suppressed by using TDI technique only if the spacecraft orbit eccentricity less than 0.003. If the requirement for eccentricity of spacecraft orbit $e < 0.003$ is too stringent, we can strive to use the second-generation TDI to suppress the laser frequency noise. The second-generation TDI have more symmetric virtual equal arm interferometric measurements than the first-generation TDI.

3. Sensitivity curve

TDI sensitivity curve as a function of Fourier frequency is defined by the square root of the density of the noise power

spectrum over the root-mean-square (RMS) of the GW response.

$$\text{sen} = \sqrt{\frac{S_i(f)}{\text{GW}_{\text{rms}}}}, \tag{14}$$

where i for α, X, P, E, and U. The expressions for $S_i(f)$ are listed in Eqs. (8)–(12). To produce the rms response for different data combinations, we assume an elliptically polarized monochromatic plane GW.[43] Two polarization states are $h_+(t) = H\sin(\Gamma)\sin(\omega t+\phi)$ and $h_\times(t) = H\cos(\Gamma)\sin(\omega t)$. Here, H characterizes the amplitude of GW, (Γ,ϕ) determine its polarization states. We average over source directions and different polarization using Monte Carlo simulations. We assume all sources are uniformly distributed on the celestial sphere and all polarization states are uniformly distributed on the Poincáre sphere in each frequency bin.

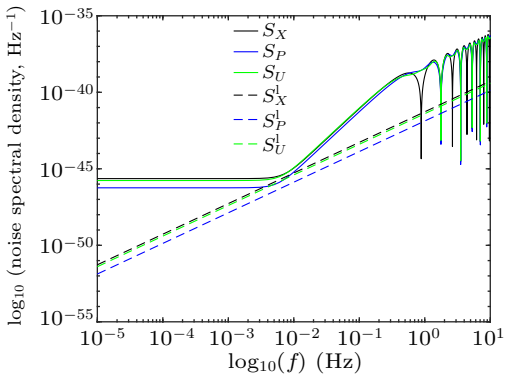


Fig. 4. The secondary noise power spectral density of TDI data combinations are higher than laser frequency noise spectral when spacecraft orbit eccentricity equals 0.001. The solid line represents the secondary noise power spectral density, the dotted line represents the laser noise spectral density.

3.1. Sensitivity curve for static detector

For a simplified model of space-borne detector, we take it as static configuration with equal arm lengths of TianQin. We can substitute the $h_+(t)$ and $h_\times(t)$ mentioned above to Eq. (1), which is a function of source directions and polarization states, e.g.,

$$\Psi_i(t) = \frac{H}{2[1-(\hat{k}\cdot\hat{n}_i)^2]}[P_i\cos(\omega t)+Q_i\sin(\omega t)], \tag{15}$$

where $P_i = \sin(\Gamma)\sin(\phi)[\sin^2(D)\cos^2(a_i-R)-\sin^2(a_i-R)]$ and $Q_i = \sin(\Gamma)\cos(\phi)[\sin^2(D)\cos^2(a_i-R)-\sin^2(a_i-R)] - 2\cos(\Gamma)\sin(a_i-R)\cos(a_i-R)\sin(D)$. The (R,D) characterize the source position. R is the angle in the detector plane between the projection of $\hat{k}$ into that plane and $\hat{n}_1$. a_i is the angle in detector plane between the unit vector $\hat{u}$ and $\hat{n}_i$.[23] We substitute Eq. (15) to different data combinations with Eq. (1). Since sensitivity curve is a function of Fourier frequency, we can directly take Fourier transform of Eq. (15) to obtain an analytic form in frequency domain. In order to obtain the average sensitivity curve, we simulate 2500 sources in each frequency bin and set the number of frequency bins are 7000 in frequency band 10^{-4} Hz–10^{1} Hz. RMS response and sensitivity curves for first generation TDI data combinations with static detector are shown with red lines in Fig. 5.

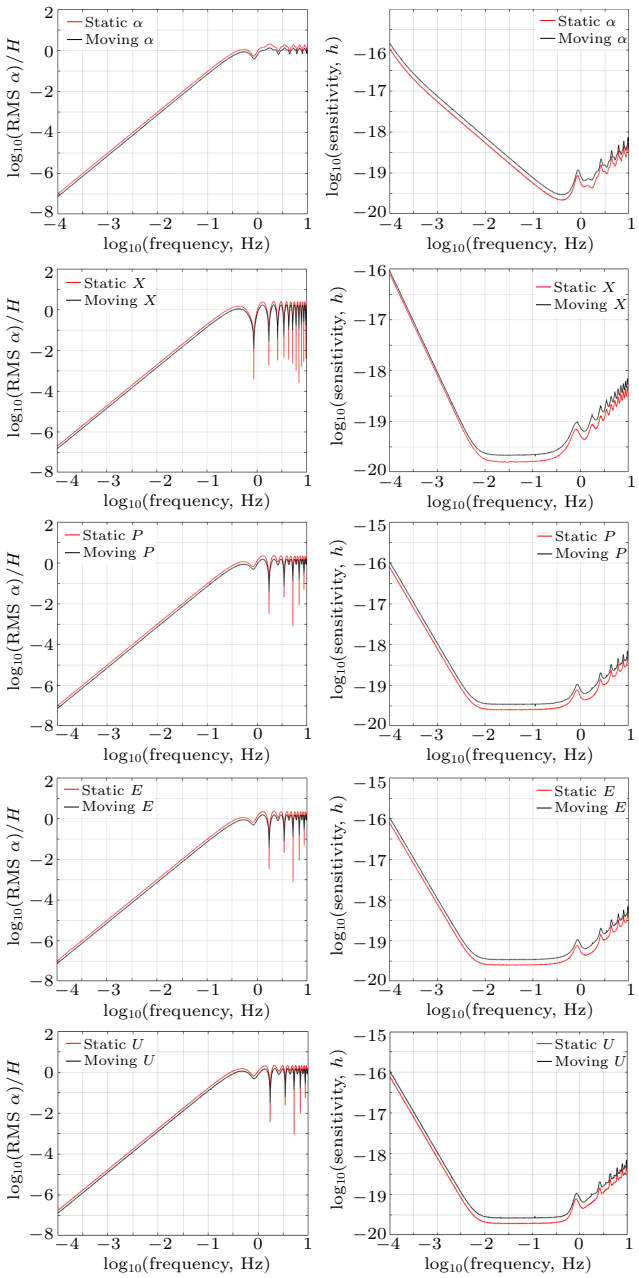


Fig. 5. Sensitivity curve for moving TianQin averaging over 1000 sources in each frequency bin. Frequency band is 10^{-4}–10^{1} Hz with 1000 frequency bins. The left panels show root-mean-square of gravitational wave response and the right panels show corresponding sensitivity curves for different TDI data combinations. The red lines represent for static cases and the moving ones with the black lines.

3.2. Sensitivity curve for moving detector

For realistic case, spacecraft configuration is not static one but rotating with time varying arm lengths. Time dependent variables are $\hat{p}_i(t)$, $l_k(t)$, and $L_k(t)$ in Eq. (1) for a moving detector. To produce the RMS response for moving detector, we can not obtain an analytical form of different data com-

binations in frequency domain directly. We need to simulate time-dependent Doppler series for each source firstly. Taking fast Fourier transform of time domain data to produce RMS response for corresponding Fourier frequency with 1000 sources in each frequency bin and the number of frequency bins are 1000 in frequency band 10^{-4} Hz–10^{1} Hz. Here, we take the observation time is 3.65 d for averaging. We use the orbit only including perturbations from the Earth and the Sun for simplification. The analytic form of TianQin orbit is referred from Ref. [44]. Explicitly, the coordinates of the n-th spacecraft in the geocentric–ecliptic coordinate system can be written as

$$\begin{aligned} p_{x_n}(t) &= R_1\big(\cos\phi_s\sin\theta_s\sin(\alpha_n-\beta')+\cos(\alpha_n-\beta')\sin\phi_s\big) \\ &\quad + R_1 e_1\Big[\frac{1}{2}\big(\cos 2(\alpha_n-\beta')-3\big)\sin\phi_s \\ &\quad + \cos(\alpha_n-\beta')\cos\phi_s\sin\theta_s\sin(\alpha_n-\beta')\Big], \\ p_{y_n}(t) &= R_1\big(\sin\phi_s\sin\theta_s\sin(\alpha_n-\beta')-\cos(\alpha_n-\beta')\cos\phi_s\big) \\ &\quad + R_1 e_1\Big[\frac{-1}{2}\big(\cos 2(\alpha_n-\beta')-3\big)\cos\phi_s \\ &\quad + \cos(\alpha_n-\beta')\sin\phi_s\sin\theta_s\sin(\alpha_n-\beta')\Big], \\ p_{z_n}(t) &= -R_1\sin(\alpha_n-\beta')\cos\theta_s \\ &\quad - R_1 e_1\cos(\alpha_n-\beta')\sin(\alpha_n-\beta')\cos\theta_s. \end{aligned} \tag{16}$$

Here e_1 is the eccentricity and $R_1 = 1.0\times10^5$ km is the semi-major axis of the spacecraft orbit. The spacecraft orbit phase α_n is

$$\alpha_n(t) = 2\pi f_{\rm sc}t + \kappa_n, \tag{17}$$

where $\kappa_n = \frac{2\pi}{3}(n-1)+\lambda$, λ is the initial orbit phase of the first $(n=1)$ spacecraft measured from $\tilde{x}$ axis, β' is the angle measured from the $\tilde{x}$ axis to the perigee of the spacecraft. $f_{\rm sc}\approx 1/(3.65\ \text{day})$ is the modulation frequency due to the rotation of the detector around the guiding center. The noise power spectrum density is corresponding to time dependent one for moving detector with changing arm-length. We also using a time averaged noise power spectrum density for each frequency bin. Take X combination for example, the remaining noise terms due to proof mass are[24]

$$\begin{aligned} X^{\rm proof\ mass} &= \hat{n}_2\cdot(-\boldsymbol{v}^*_{1,2233}+\boldsymbol{v}^*_{1,22}-\boldsymbol{v}^*_{1,33} \\ &\quad +\boldsymbol{v}^*_1+2\boldsymbol{v}_{3,233}-2\boldsymbol{v}_{3,2}) \\ &\quad +\hat{n}_3\cdot(-\boldsymbol{v}_{1,2233}+\boldsymbol{v}_{1,33}-\boldsymbol{v}_{1,22} \\ &\quad +\boldsymbol{v}_1+2\boldsymbol{v}^*_{2,223}-2\boldsymbol{v}^*_{2,3}). \end{aligned} \tag{18}$$

The power spectrum density for acceleration noise with unequal time varying arm length is

$$\begin{aligned} S_X^{\rm proof\ mass} &= \big[8\sin^2[2\pi f(L_2-L_3)]+8\sin^2[2\pi f(L_2+L_3)] \\ &\quad +32\sin^2(2\pi fL_3)\big]\cdot S_y^{\rm pm}. \end{aligned} \tag{19}$$

On the other hand, the power spectrum density for optical path noise is

$$S_X^{\rm optical\ path} = \Big[8\sin^2(2\pi fL_3)+8\sin^2(2\pi fL_2)\Big]\cdot S_y^{\rm op}. \tag{20}$$

The resulting noise power spectrum density for combination X with moving detector is

$$\begin{aligned} S_X(f,t) &= \big[8\sin^2[2\pi f(L_2-L_3)]+8\sin^2[2\pi f(L_2+L_3)] \\ &\quad +32\sin^2(2\pi fL_3)\big]\cdot S_y^{\rm pm} \\ &\quad +\big[8\sin^2(2\pi fL_3)+8\sin^2(2\pi fL_2)\big]\cdot S_y^{\rm op}. \end{aligned} \tag{21}$$

This equation equals Eq. (10) when $L_2 = L_3 = L$ for static constellation. Power spectrum density for data combination α, P, E, and U can also give using the same method. The RMS response and sensitivity curve results are shown with black lines in Fig. 5.

Sensitivity curves comparison between static and moving detector are shown in Fig. 5. The red lines represent static case and the black lines represent moving case. Sensitivity curves for moving detector are less sensitive than static ones for all TDI data combinations. The reason is that dynamic constellations have a pool GW response under the same secondary noise budget. In other words, the first generation TDI data combinations can only cancel the unequal arm length up to zero order of magnitude.[45] However, the moving detector with less sensitive does not satisfy this condition and the first generation TDI cannot cancel the arm-length up to higher orders of magnitude. A more robust illustration to this issue can refer to Ref. [30].

4. Principle component analysis

A different approach to TDI is called principle component analysis which can generate the same data combinations without laser phase noise at specific times. PCA is usually used to reduce the dimensionality of a problem by decomposing the data into an orthogonal basis whose vectors are called principal components in statistics. Then, one keeps only the vectors that contain the most information about the data by restricting the analysis to the components having the largest variance. In this way, we can cancel laser phase noise only according to the total noise covariance matrix. In fact, PCA is a linear transform by diagonalizing covariance matrix, which makes the biggest variance on the first axis, the second biggest variance on the second axis, etc. Conducting data analysis-based PCA method can dramatically reduce the dimension of the data to simplify our high dimension space problem in this fully new orthogonalized coordinate. We can choose coordinate with principle component to do data analysis and keep the most information about the original data. Romano and Woan showed that PCA identified a linear combination of the data

streams that did not depend on the laser noise that was common to TDI technique. We use the principle and notation as Ref. [37]. Here p_i is the frequency noise associated with the two lasers (assumming that laser phase to be locked on each spacecraft) on spacecraft i. We take σ_p^2 and σ_n^2 for the variance of laser phase noise and the variance of the secondary noise. Of course, we have inequality $\sigma_p^2 \gg \sigma_n^2$ in this case. Six time series data only including laser phase noise and the secondary noise at any time stamps t

$$
\begin{aligned}
s_1[t] &= p_2[t-L_3] - p_1[t] + n_1[t], && (22)\\
s_{1'}[t] &= p_3[t-L_2] - p_1[t] + n_{1'}[t], && (23)\\
s_2[t] &= p_3[t-L_1] - p_2[t] + n_2[t], && (24)\\
s_{2'}[t] &= p_1[t-L_3] - p_2[t] + n_{2'}[t], && (25)\\
s_3[t] &= p_1[t-L_2] - p_3[t] + n_3[t], && (26)\\
s_{3'}[t] &= p_2[t-L_1] - p_3[t] + n_{3'}[t]. && (27)
\end{aligned}
$$

The dimension of the noise covariance C total depends on observation time T, e.g., $\alpha = 1, 2, 3, 4, 5$. Covariance matrix is thus a 30×30 matrix, whose $\alpha\beta$-th element is itself a 6×6 matrix:

$$
C_{\alpha\beta} = \begin{pmatrix}
\langle s_1[\alpha] s_1[\beta]\rangle & \langle s_1[\alpha] s_{1'}[\beta]\rangle & \cdots \\
\langle s_{1'}[\alpha] s_1[\beta]\rangle & \langle s_{1'}[\alpha] s_{1'}[\beta]\rangle & \cdots \\
\langle s_2[\alpha] s_1[\beta]\rangle & \langle s_2[\alpha] s_{1'}[\beta]\rangle & \cdots \\
\langle s_{2'}[\alpha] s_1[\beta]\rangle & \cdot & \cdots \\
\langle s_3[\alpha] s_1[\beta]\rangle & \cdot & \cdots \\
\langle s_{3'}[\alpha] s_1[\beta]\rangle & \cdot & \cdots
\end{pmatrix}. \quad (28)
$$

Here, σ_p^2 is the variance of laser phase noise, and σ_n^2 is the variance of the secondary noise. The relationship between laser phase noise and the secondary noise at different time stamps are

$$
\begin{aligned}
\langle n_i[\alpha] n_j[\beta]\rangle &= \langle n_i'[\alpha] n_j'[\beta]\rangle = \delta_{\alpha\beta}\delta_{ij}\sigma_n^2, && (29)\\
\langle p_i[\alpha] p_j[\beta]\rangle &= \delta_{\alpha\beta}\sigma_p^2, && (30)\\
\langle n_i[\alpha] n_j'[\beta]\rangle &= \langle n_i[\alpha] p_j[\beta]\rangle = \langle n_i'[\alpha] p_j[\beta]\rangle = 0. && (31)
\end{aligned}
$$

4.1. Covariance matrix for static detector

The TianQin toy model features a triangular configuration with static and constant arm lengths. Samples of covariance matrix with sample times $t = 0, 1, 2, \ldots, 9$ and with equal arm lengths ($L = 3, 3, 3$) and unequal arm lengths ($L = 2, 3, 4$) are shown in Fig. 6. In comparison with the unequal arm lengths case, the number of diagonals is the same but with more values in each block, that is, the density of the blocks has increased. On the other hand, the number of correlations in the other diagonals has also increased for unequal arm lengths. We can also get the same TDI variables using combinations of the eigenvectors from covariance matrix based on the first generation TDI. This part is not included in this paper, but can be found in Ref. [30]. We also show that the same results for the second generation TDI and PCA method in Section 5.

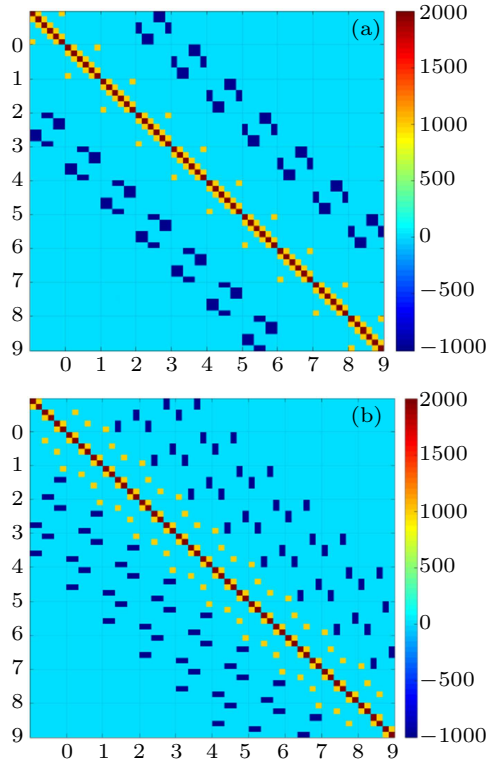


Fig. 6. The covariance matrix for times $t = 0, 1, 2, \ldots, 9$, and with equal arm lengths (top, $L = 3, 3, 3$) and unequal arm lengths (bottom, $L = 2, 3, 4$). We also assume the variances for phase noise and the secondary noise are $\sigma_p^2 = 1000$ and $\sigma_n^2 = 1$.

4.2. Covariance matrix for moving detector

TianQin will have time varying arm lengths in a realistic case with earth modulation frequency of one over a year around the Sun. On the other hand, spacecraft modulation

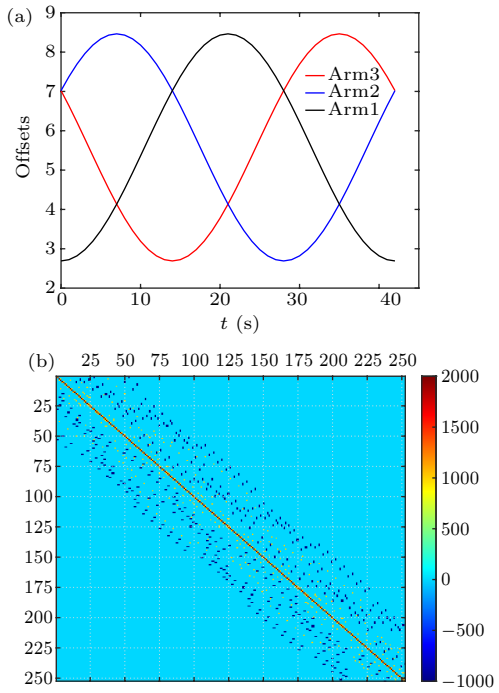


Fig. 7. Sample covariance matrix for time varying arm lengths for TianQin. We assumed three phases are locked on each spacecraft. Three different arm lengths were used as the model as left figure. We also assume the variances for phase noise and the secondary noise are $\sigma_p^2 = 1000$ and $\sigma_n^2 = 1$.

frequency is $1/(3.65\ \text{days})$ around the Earth. In order to illustrate this modulation in a small matrix, the initial separations between the arm lengths and their periods are exaggerated. Many time stamps are dropped out for this time varying arm length model. The mean arm length of TianQin is approximately 0.57 s. The sampling time is 1 s and the covariance matrix for moving TianQin are shown in Fig. 7. The block density of the covariance matrix is not widely distributed as LISA case[39] with 4-s initial offsets.

We also compare the covariance matrix between static but with unequal arm length ($L = 2,\ 3,\ 4$) and moving case with the same observation times ($t = 0,\ 1,\ 2,\ \ldots,\ 9$) in Fig. 8. They have the same maximum variance but with different minimum variances. Matrix aggregation is higher near the diagonal for moving TianQin because the sampling time is only 1 s. However, the left panel represents unequal arm lengths ($L = 2,\ 3,\ 4$) and the arm lengths are much lager than realistic TianQin.

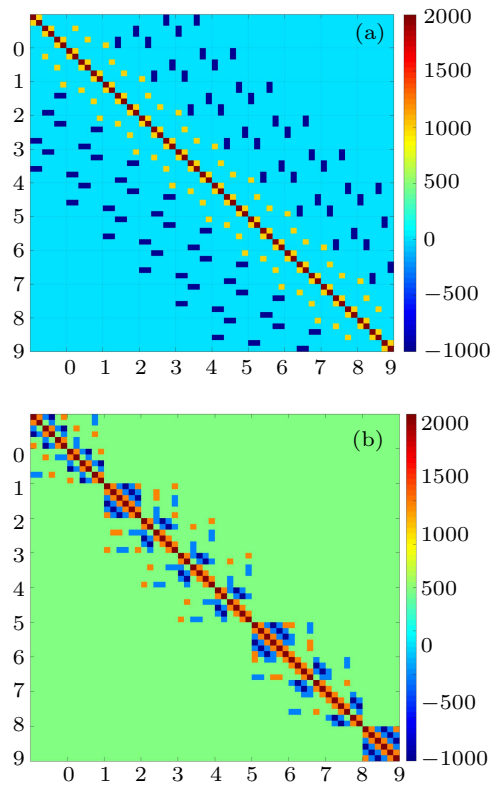


Fig. 8. Covariance matrix comparison between static but with unequal arm length (top, $L = 2,\ 3,\ 4$) and moving detector (bottom) with the same observation times. We also assume the variances for phase noise and the secondary noise are $\sigma_p^2 = 1000$ and $\sigma_n^2 = 1$.

5. Relationship between TDI and PCA

TDI variables are suitable for continues time series but PCA can generate the same combination at specific times. The properties of PCA at specific times which may be important for gap observations. The relationship between first generation and PCA has been demonstrated by Romano and Woam.[37] One can show that the Sagnac combination for spacecraft 1 (denoted $\alpha(t)$ in Ref. [21]) is a linear combination of eigenvectors: $-\hat{e}_4 - \hat{e}_7 - \hat{e}_8$. Explicitly,

$$\alpha(5) \equiv s_{1'}(5) + s_{3'}(3) + s_{2'}(2) - s_1(5) - s_2(2) - s_3(1), \quad (32)$$

which is just the discretised-version of

$$\begin{aligned}\alpha(t) \;=\; & s_{1'}(t) + s_{3'}(t - L_2) + s_{2'}(t - L_1 - L_2) \\ & - s_1(t) - s_2(t - L_3) - s_3(t - L_1 - L_3),\end{aligned} \quad (33)$$

appropriate for the arm lengths assumption. Here we concentrate on the second generation TDI and PCA method. First of all, we can write the second generation $\alpha_1(t)$ combination:

$$\begin{aligned}\alpha_1(t) \;=\; & s_1(t) + s_2(t - L_3) + s_3(t - L_1 - L_3) \\ & + s_{1'}(t - L_2 - L_1 - L_3) + s_{3'}(t - L_2 - L_2 - L_1 - L_3) \\ & + s_{2'}(t - L_1 - L_2 - L_2 - L_1 - L_3) \\ & - s_3(t - L_1 - L_3 - L_3 - L_1 - L_2) \\ & - s_2(t - L_3 - L_3 - L_1 - L_2) - s_1(t - L_3 - L_1 - L_2) \\ & - s_{2'}(t - L_1 - L_2) - s_{3'}(t - L_2) - s_{1'}(t).\end{aligned} \quad (34)$$

Using the same assumptions for arm lengths with $L_1 = 1$, $L_2 = 2$, $L_3 = 3$. If the covariance matrix is restricted to positive values, the only time that will have offsets occurring with all these values is $t = 11$. The values for α_1 combination is

$$\begin{aligned}\alpha_1(11) \;=\; & s_1(11) + s_2(8) + s_3(7) + s_{1'}(5) + s_{3'}(3) \\ & + s_{2'}(2) - s_3(1) - s_2(2) - s_1(5) \\ & - s_{2'}(8) - s_{3'}(9) - s_{1'}(11).\end{aligned} \quad (35)$$

In order to generate the same result as TDI combination, we calculate the eigenvalues and eigenvectors of 66×66 covariance matrix. There are 40 distinct eigenvalues, the smallest of which is independent of laser phase noise. This minimal eigenvalue

$$\lambda_{\min} = \sigma_n^2 \quad (36)$$

is 27-fold degenerate. Here we only show five eigenvectors that used to generate the same combinations as the second generation $\alpha_1(11)$. The solution for the second generation is $\alpha_1(11) = -\hat{e}_3 - \hat{e}_7 - \hat{e}_{11} + \hat{e}_{21} + \hat{e}_{27}$. The results for five eigenvectors are

$$\begin{aligned}\hat{e}_3 \;=\; & s_{3'}(3) + s_2(4) - s_1(5) + s_1(7) - s_3(7) \\ & - s_2(8) + s_3(9) - s_1(11) + s_{1'}(11), \quad (37) \\ \hat{e}_7 \;=\; & -s_{3'}(3) - s_2(4) + s_1(5) - s_1(7) \\ & + s_3(7) + s_2(8) - s_3(9) + s_{3'}(9), \quad (38) \\ \hat{e}_{11} \;=\; & -s_3(7) - s_2(8) + s_{2'}(8), \quad (39) \\ \hat{e}_{21} \;=\; & s_{3'}(3) - s_1(5) + s_{1'}(5), \quad (40) \\ \hat{e}_{27} \;=\; & -s_3(1) - s_2(2) + s_{2'}(2), \quad (41)\end{aligned}$$

which give

$$-(\hat{e}_3 + \hat{e}_7) \;=\; -[s_{3'}(3) + s_2(4) - s_1(5) + s_1(7) - s_3(7)$$

$$
\begin{aligned}
&-s_2(8)+s_3(9)-s_1(11)+s_{1'}(11)\\
&+(-s_{3'}(3)-s_2(4)+s_1(5)-s_1(7)\\
&+s_3(7)+s_2(8)-s_3(9)+s_{3'}(9))]\\
=\ &-s_{3'}(9)+s_1(11)-s_{1'}(11), \qquad (42)
\end{aligned}
$$

and we have

$$
\begin{aligned}
&-(\hat{e}_3+\hat{e}_7)-\hat{e}_{11}+\hat{e}_{21}+\hat{e}_{27}\\
=\ &-s_{3'}(9)+s_1(11)-s_{1'}(11)+s_3(7)+s_2(8)-s_{2'}(8)\\
&+s_{3'}(3)-s_1(5)+s_{1'}(5)-s_3(1)-s_2(2)+s_{2'}(2)\\
\equiv\ &\alpha_1(11). \qquad (43)
\end{aligned}
$$

In fact, eigenvectors can be written in different form due to its non-uniqueness. Finally, the same TDI variables can be obtained from eigenvectors combination although eigenvectors express in different forms. Therefore, TDI variables is a consequence of principle component analysis with eigenvectors combination of covariance matrix at specific time stamps.

6. Discussion and conclusion

Although we initially considered a simplified toy model of a space-borne detector, it provides valuable guidance for the real cases. The sensitivity curve for a static configuration has roughly the same sensitivity structure as for a moving one. From sensitivity curve showed above, we can find that combination X is more sensitive to gravitational wave. TianQin will be more sensitive in high frequency band than LISA because of shorter arm length. It is possible to combine with ground-based detectors to do multi-messenger observations. In this paper, we obtained sensitivity curve based on analytic orbit only including perturbations form the Sun and the Earth for TianQin. We can consider a more realistic and optimized orbit of TianQin[46] which considering the perturbations from seven planets and the Moon. Here, we average over 1000 sources. More sources needed to averaging in next step using optimized algorithm or using parallel computing. A package that is very similar with LISACode or LISASynthetic for TianQin is expected to be established in the near future. With this package, we can get sensitivity curves for different TDI data combinations, simulate TDI data for different kinds of gravitational wave sources which used for mock TianQin data analysis. This is an important segment for a large project to be implemented step by step.

In Section 4, we showed covariance matrix for static and moving TianQin. Besides, time varying arm length model for TianQin with a large spacecraft modulation frequency and initially separated for large offsets that is not real case due to large dimension of the matrix. More realistic case should be considered with principle component analysis. In Section 5, we give the relationship between PCA and the second generation of TDI. As indicated in Ref. [37], the reduced set of eigen-streams is sufficient basis (and possibly more than sufficient) to carry out all possible astronomy with TianQin.

Acknowledgements

Project supported by "GrEAT network" in School of Physics and Astronomy, University of Glasgow. Wang Y gratefully acknowledges support from the National Key Research and Development Program of China (Grant Nos. 2023YFC2206702 and 2022YFC2205201), and the Major Science and Technology Program of Xinjiang Uygur Autonomous Region of China (Grant No. 2022A03013-4). Hu X C is supported by the Tongling University Talent Program (Grant No. 2021tlxyrc26) and Tongling University Natural Science Research Project (Grant No. 2024tlxykjZD10).

References

[1] Harry G M and LIGO Scientific Collaboration 2010 *Classical and Quantum Gravity* **27** 084006
[2] LIGO Scientific Collaboration, Aasi J, Abbott B P, Abbott R, Abbott T, Abernathy M R, Ackley K, *et al.* 2015 *Classical and Quantum Gravity* **32** 074001
[3] Acernese F, Agathos M, Agatsuma K, Aisa D, Allemandou N, *et al.* 2015 *Classical and Quantum Gravity* **32** 024001
[4] Somiya K 2012 *Classical and Quantum Gravity* **29** 124007
[5] Amaro-Seoane P, Audley H, Babak S, Baker J, Barausse E, Bender P, Berti E, Binetruy P, Born M, Bortoluzzi D, Camp J, Caprini C, *et al* 2017 arXiv e-prints arXiv: 1702.00786
[6] eLISA Consortium, Amaro Seoane P, Aoudia S, Audley H, Auger G, Babak S, Baker J, Barausse E, Barke S, Bassan M, Beckmann V, Benacquista M, Bender P L, Berti E, *et al.* 2013 arXiv e-prints arXiv: 1305.5720
[7] Armano M, Audley H, Auger G, Baird J T, Bassan M, Binetruy P, Born M, Bortoluzzi D, Brandt N, Caleno M, Carbone L, Cavalleri A, *et al.* 2016 *Phys. Rev. Lett.* **116** 231101
[8] Luo J, Chen L S, Duan H Z, Gong Y G, Hu S, Ji J, Liu Q, Mei J, Milyukov V, Sazhin M, Shao C G, Toth V T, Tu H B, Wang Y, Wang Y, Yeh H C, Zhan M S, Zhang Y, Zharov V and Zhou Z B 2016 *Classical and Quantum Gravity* **33** 035010
[9] Conklin J W, Buchman S, Aguero V, Alfauwaz A, Aljadaan A, Almajed M, Altwaijry H, Al-Saud T, Balakrishnan K, Byer R L, Bower K, Costello B, Cutler G D, DeBra D B, Faied D M, Foster C, Genova A L, Hanson J, Hooper K, Hultgren E, Jaroux B, Klavins A, Lantz B, Lipa J A, Palmer A, Plante B, Sanchez H S, Saraf S, Schaechter D, Sherrill T, Shu K L, Smith E, Tenerelli D, Vanbezooijen R, Vasudevan G, Williams S D, Worden S P, Zhou J and Zoellner A 2011 arXiv e-prints arXiv: 1111.5264
[10] Tinto M, de Araujo J C N, Aguiar O D and Alves M E S 2013 *Astroparticle Physics* **48** 50
[11] Tinto M, DeBra D, Buchman S and Tilley S 2015 *Rev. Sci. Instrum.* **86** 014501
[12] Hiscock B and Hellings R W 1997 *OMEGA: A space gravitational wave MIDEX mission.* Vol. 29
[13] Ni W T 2002 *Int. J. Mod. Phys. D* **11** 947
[14] Ni W T, Cao J, Dittus H, Dong P, Guo J, Lämmerzahl C, Mei X, Shaul D, Sumner T J, Wang G, Hou X, Huang C G, Meng J, Wang H, Zhang C and Zhang Y 2010 38*th COSPAR Scientific Assembly* **38** 11
[15] Gong X, Lau Y K, Xu S, Amaro-Seoane P, Bai S, Bian X, Cao Z, Chen G, Chen X, Ding Y, Dong P, Gao W, Heinzel G, Li M, Li S, Liu F, Luo Z, Shao M, Spurzem R, Sun B, Tang W, Wang Y, Xu P, Yu P, Yuan Y, Zhang X and Zhou Z 2015 *J. Phys.: Conf. Ser.* **610** 012011
[16] Cutler C and Harms J 2006 *Phys. Rev. D* **73** 042001
[17] Crowder J and Cornish N J 2005 *Phys. Rev. D* **72** 083005
[18] Sato S, Kawamura S, Ando M, *et al.* 2009 *J. Phys.: Conf. Ser.* **154** 012040
[19] Ni W T 2016 *Int. J. Mod. Phys. D* **25** 1630001

[20] Bender P, Brillet A, Ciufolini I, Cruise A, Cutler C, Danzmann K, Fidecaro F, *et al.* 1998 *LISA Mission Concept Study, Laser Interferometer Space Antenna for the Detection and Observation of Gravitational Waves*, Vol. 233 (MPQ)
[21] Tinto M and Dhurandhar S V 2014 *Living Reviews in Relativity* **17** 6
[22] Tinto M and Armstrong J W 1999 *Phys. Rev. D* **59** 102003
[23] Armstrong J W, Estabrook F B and Tinto M 1999 *The Astrophysical Journal* **527** 814
[24] Estabrook F B, Tinto M and Armstrong J W 2000 *Phys. Rev. D* **62** 042002
[25] Armstrong J W, Estabrook F B and Tinto M 2001 *Classical and Quantum Gravity* **18** 4059
[26] Tinto M, Armstrong J W and Estabrook F B 2001 *Classical and Quantum Gravity* **18** 4081
[27] Prince T A, Tinto M, Larson S L and Armstrong J W 2002 *Phys. Rev. D* **66** 122002
[28] Zhang C, Gao Q, Gong Y, Liang D, Weinstein A J and Zhang C 2019 *Phys. Rev. D* **100** 064033
[29] Tinto M and Hartwig O 2018 *Phys. Rev. D* **98** 042003
[30] Vallisneri M 2005 *Phys. Rev. D* **71** 022001
[31] Nayak K R and Vinet J Y 2004 *Phys. Rev. D* **70** 102003
[32] Shaddock D A 2004 *Phys. Rev. D* **69** 022001
[33] Shaddock D A, Tinto M, Estabrook F B and Armstrong J W 2003 *Phys. Rev. D* **68** 061303
[34] Tinto M, Shaddock D A, Sylvestre J and Armstrong J W 2003 *Phys. Rev. D* **67** 122003
[35] Dhurandhar S V, Nayak K R and Vinet J Y 2002 *Phys. Rev. D* **65** 102002
[36] Tinto M, Estabrook F B and Armstrong J W 2002 *Phys. Rev. D* **65** 082003
[37] Romano J D and Woan G 2006 *Phys. Rev. D* **73** 102001
[38] Abdi Hervé W L J 2010 *Principal Component Analysis*, Vol. 2 (WIREs Comp Stat)
[39] Leighton M D 2016 *A principal component approach to space-based gravitational wave astronomy* Thesis (phd) University of Glasgow
[40] Baghi Q, Thorpe J I, Slutsky J and Baker J 2021 *Phys. Rev. D* **103** 042006
[41] Baghi Q, Baker J, Slutsky J and Thorpe J I 2021 *Phys. Rev. D* **104** 122001
[42] Wang G and Ni W T 2012 *Chinese Astronomy and Astrophysics* **36** 211
[43] Armstrong J W, Estabrook F B and Tinto M 2001 *Classical and Quantum Gravity* **18** 4059
[44] Hu X C, Li X H, Wang Y, Feng W F, Zhou M Y, Hu Y M, Hu S C, Mei J W and Shao C G 2018 *Classical and Quantum Gravity* **35** 095008
[45] Vallisneri M 2005 *Phys. Rev. D* **72** 042003
[46] Ye B B, Zhang X, Zhou M Y, Wang Y, Yuan H M, Gu D, Ding Y, Zhang J, Mei J and Luo J 2019 *Int. J. Mod. Phys. D* **28** 1950121